Acoustically shaped laser: a machining tool for Industry 4.0

Salvatore Surdo[1], Alessandro Zunino[1,2], Alberto Diaspro[1,2], Martí Duocastella[1,3]

[1] *Nanoscopy, CHT Erzelli, Istituto Italiano di Tecnologia, Via Enrico Melen 83, Building B, 16152 Genova, Italy*
[2] *Department of Physics, University of Genoa, Via Dodecaneso 33, 16146 Genova, Italy*
[3] *Departament de Física Aplicada, Universitat de Barcelona, C/Martí i Franquès 1, 08028 Barcelona, Spain*

ABSTRACT
The high versatility of laser direct-write (LDW) systems offers remarkable opportunities for Industry 4.0. However, the inherent serial nature of LDW systems can seriously constrain manufacturing throughput and, consequently, the industrial scalability of this technology. Here we present a method to parallelise LDWs by using acoustically shaped laser light. We use an acousto-optofluidic (AOF) cavity to generate acoustic waves in a liquid, causing periodic modulations of its refractive index. Such an acoustically controlled optical medium diffracts the incident laser beam into multiple beamlets that, operating in parallel, result in enhanced processing throughput. In addition, the beamlets can interfere mutually, generating an intensity pattern suitable for processing an entire area with a single irradiation. By controlling the amplitude, frequency, and phase of the acoustic waves, customised patterns can be directly engraved into different materials (silicon, chromium, and epoxy) of industrial interest. The integration of the AOF technology into an LDW system, connected to a wired-network, results into a cyber-physical system (CPS) for advanced and high-throughput laser manufacturing. A proof of concept for the computational ability of the CPS is given by monitoring the fidelity between a physical laser-ablated pattern and its digital avatar. As our results demonstrate, the AOF technology can broaden the usage of lasers as machine tools for industry 4.0.

Corresponding authors: Salvatore Surdo, e-mail: salvatore.surdo@iit.it, Martí Duocastella, e-mail: marti.duocastella@iit.it

1. INTRODUCTION

The fourth industrial revolution or Industry 4.0 (I4) exploits machines that are augmented by means of internet connections and sensor networks and are controlled by intelligent systems capable of monitoring the entire production chain and making autonomous decisions [1], [2]. This enables workpiece production with high levels of adaptability in terms of manufacturing conditions and design adjustments, which ultimately results in high-quality manufacturing at high yields [3], [4]. In detail, the I4 paradigm encompasses technologies that belong to two broad categories, often known as digital and physical worlds. The former includes the Internet of Things (IoT), big data, and cloud computing and allows wireless collection of data from physical objects (sensors, machines, and products) as well as their real-time processing, and is aimed at improving production and logistics efficiency. The second group comprises robots and manufacturing tools that are digitally controlled and perform machining operations that are capable of shaping materials according to a specific design.

Over the past few decades, significant efforts have been directed toward the growth of the digital world, which currently offers multiple IoT elements (sensors, actuators, and nodes) [5], [6] and wireless communication protocols such as Zigbee, 5G, and LTE [7]-[9]. The physical world can now include autonomous robots, although it is still looking for a suitable manufacturing method, often referred to as a 'machine tool 4.0' (MT4.0) [10]. The ideal candidate should be capable of performing multiple operations, such as the cutting, punching, forming, and welding of a large range of functional materials, ideally at high speed and with design flexibility. However, traditional tools only fulfil a few of these requests. For instance, computer numerical control (CNC) milling machines can cut several materials, such as wood, metals, plastics, glass, and foams, but operate only in subtractive mode, typically with one material at a time, and suffer from mechanical wear issues. Their additive counterparts, such as fused deposition modelling and ink-jet printing, are significantly more flexible in pattern selection but typically operate with a reduced number of materials; their compatibility with metals, arguably the most widely used

resource in industry, is limited [11], [12]. Recent attempts to address these issues with hybrid systems that combine additive and subtractive methods have led to complex machine tools with limited speed and high costs [13].

A family of technologies capable of solving the problems encountered with traditional methods is laser direct writing (LDW) [14]. LDW can use a laser beam to either alter a controlled volume of material causing localised damage to a surface (subtractive operation) or can transfer a specified amount of material onto a workpiece (additive operation). In both cases, the desired pattern is first drawn with computer-aided design (CAD) and then sequentially etched or built by scanning the sample with the laser beam. These peculiarities make LDW a good choice as a machine tool for I4 [15]. LDW is compatible with metals [16], ceramics [17], polymers [18], and more exotic materials such as wood [19] and leather [20]. Furthermore, being capable of both subtractive and additive operations, LDW can implement multiple machining processes, such as printing [21], depositing [22], the joining [23] of various materials, and the polishing [24], coating [25], and cleaning [26] of a surface. Finally, lasers are controlled numerically and can be connected to other physical or digital objects, enabling the realisation of laser-based cyber-physical systems (CPSs) for advanced manufacturing.

So far, the application of LDW in I4 is limited to a few operations, namely laser ablation and sintering, and the reasons can be ascribed to its serial nature and limited flexibility and speed in terms of beam shape selection, which limit the manufacturing throughput. These constraints have spurred the development of methods for shaping a laser beam in a tuneable and controlled way. Examples include laser beam parallelisation

with passive optical elements (gratings [27] and beams splitters [28]) or beam shaping by means of mask projection systems [29]. However, these methods lack tunability in terms of the number, position, and shape of the laser beams, thus impeding the real-time correction and adjustment of the manufacturing process. This problem can be solved with active optical elements such as digital micromirror devices (DMD) [30] and spatial light modulators (SLM) [31] that allow for the generation of tuneable light patterns; however, they suffer from pixellation issues and long response times and can be easily damaged.

We recently proved that rapid (in the sub-microsecond timescale) both-beam parallelisation (up to 35 beams) and the generation of complex and tuneable light patterns can be achieved through the interaction of laser and acoustic waves in a liquid [32], [33]. Our technology, acousto-optofluidics (AOF), enables high-throughput material processing without suffering from the problems (damage, pixellation, and speed) of conventional methods. Here, we present a detailed characterisation of the acousto-optofluidic cavity and the first results of its integration into an LDW system, aimed at proving its feasibility as a machine tool for I4. Specifically, we illustrate a simple (two-level) laser-based CPS with AOF functionalities for the high throughput additive and subtractive machining of various materials such as metals, polymers, and semiconductors.

2. ACOUSTICALLY SHAPED LASER BEAM

2.1. Acoustic cavity: design, implementation, and characterisation

The key element of our technology is an acoustic resonant cavity capable of inducing stationary pressure waves in a liquid. Figure 1 a) shows a schematic of the cavity that encompasses two
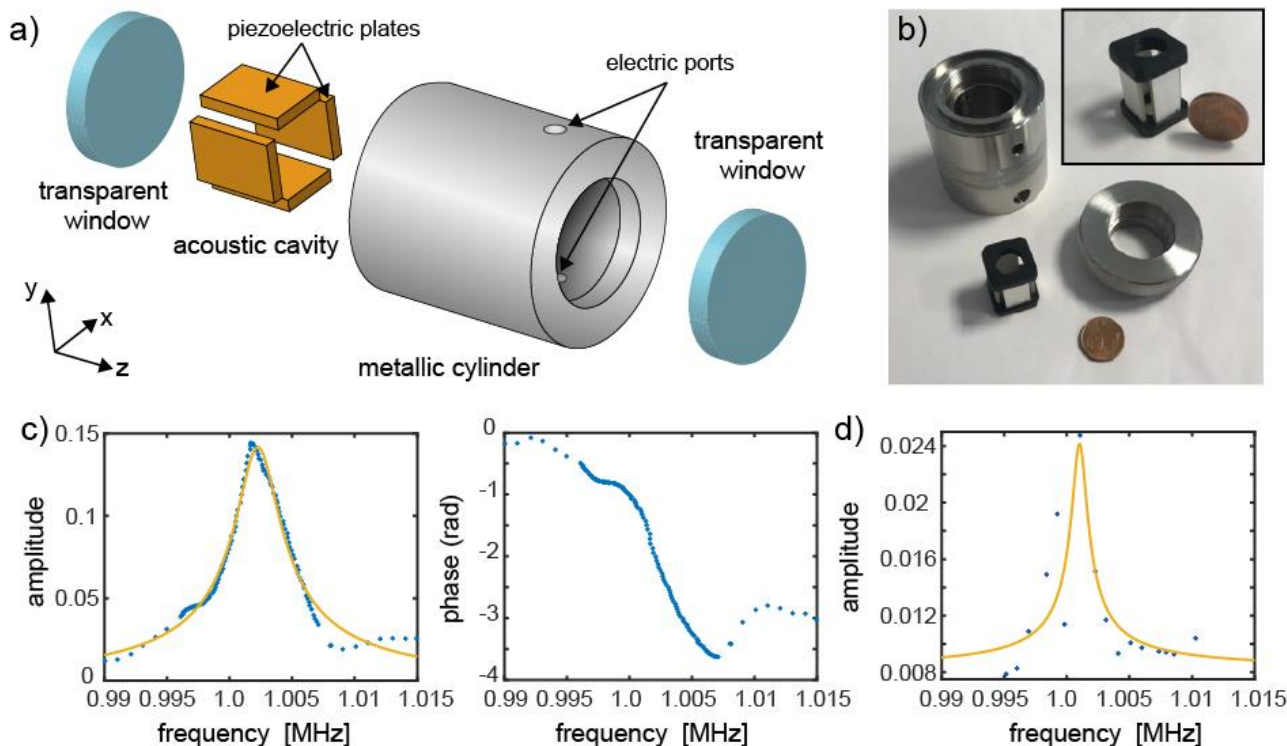
Figure 1. Implementation and characterisation of the acoustic cavity. a) Schematic description of the main components of the AOF cavity, which consists of four rectangular (2 cm × 1 cm) piezoelectric plates, a metallic cylindrical container (∅ = 2.54 cm), and two circular glass windows. b) Optical images of a disassembled AOF cavity. The inset shows a magnified view of the piezoelectric plates, assembled according to rectangular symmetry. c) Transfer functions (amplitude and phase) of the cavity. d) Crosstalk (amplitude) between the X- and Y-axis of the cavity. The blue symbols denote the experimental data, while the yellow lines are the best-fit resonance functions.

couples of rectangular piezoelectric plates, with each pair being perpendicular to the other. The cavity is placed in a metallic cylinder and two glass circular windows seal the device with the help of O-rings. The two holes in the cylinder are for electrical connections between the piezoelectric elements and external instrumentation (waveform generator and amplifier). Figure 1 b) shows an optical image of the main components of the cavity, which has a final size of 2 cm^3.

The application of sinusoidal signals to the piezoelectric pair generates vibrations in the liquid. Propagation of these acoustic waves along the X- and Y-axes can be described by solving the damped acoustic wave equation with appropriate boundary conditions [33], [34]. On resonance, standing acoustic and, hence, density waves are present in the cavity at resonant frequencies given by the following equation:

$$f_{\mathrm{r}} = m \, \frac{c_{\mathrm{s}}}{2 \, w}, \tag{1}$$

where c_{s} is the speed of sound in the liquid ($c_{\mathrm{s}} = 1490$ m/s in water at room temperature), $w = 1$ cm is the distance between the piezoelectric plates of each couple, and m is an odd integer that identifies the resonance cavity order. Figure 1 c) shows the measured transfer function for both amplitude and phase between the piezoelectric plates of the same couple. A resonance is clearly visible at $f_{\mathrm{r}} \approx 1$ MHz that corresponds to the 13$^{\mathrm{th}}$ harmonic. Notably, the resonance has a good quality factor ($Q \approx 290$), which helps to filter out undesired contributes such as noise and environmental signals. Interestingly, the crosstalk, namely the transfer function between the piezoelectric plates of different pairs, has also a peak at such a resonant frequency but with a significantly smaller amplitude – roughly one order of magnitude (see Figure 1. d).

2.2. Laser diffraction through the acoustic cavity

The previous section enables the prediction of the resonant conditions for the cavity and the driving frequencies of the piezoelectric plates that result in standing acoustic waves in the liquid. What remains is understanding how the laser beam that travels through the cavity (along the Z-axis) is diffracted by sound. To shed light on this point, we must first determine how the stationary acoustic waves alter the refractive index of the liquid. On resonance, the induced vibrations cause a periodic modulation of the density of the liquid, which, according to the Lorentz–Lorenz model, translates into a periodic refractive index that can be calculated with [33]:

$$n(x,t) = n_0 + \Delta n \cos(2 \, \pi \, f_{\mathrm{r}} \, t) \cos\left(\frac{2 \, \pi \, f_{\mathrm{r}}}{c_{\mathrm{s}}} x\right), \tag{2}$$

where n_0 is the static refractive index of the liquid and Δn the peak of the induced variations. The latter depends on both the amplitude and frequency of the driving signals [32], [33]. Based on Equation 2, we can anticipate that the cavity behaves as an oscillating periodic grating capable of diffracting the incident light. Specifically, Figure 2 shows the effects of the AOF cavity on a Gaussian laser beam when combined with a telescope. In the focal plane of the first lens, the oscillating grating diffracts the laser beam into multiple beamlets [32]. The number, spacing, and intensity of each diffracted spot can be controlled by properly adjusting the driving parameters, such as amplitude, frequency, and the phase of the signals applied to the piezoelectric plates. As such, the AOF cavity enables laser parallelisation, provides an enhancement in the throughput roughly equal to the number of spots, and is only limited by the energy of the laser.
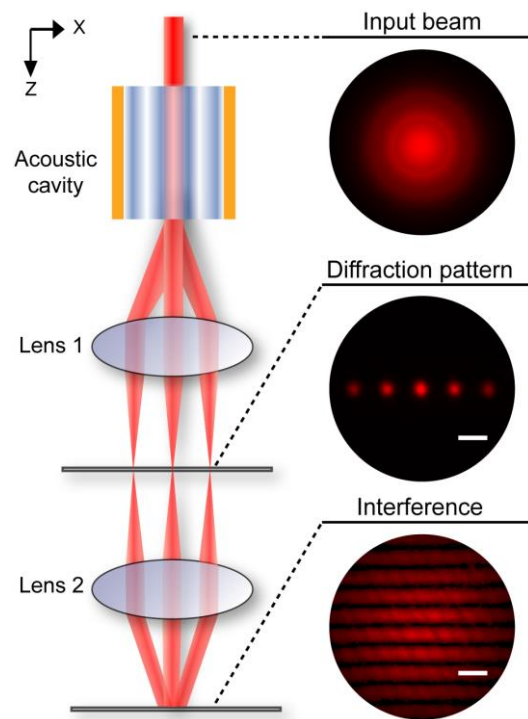
Figure 2. The optical setup used to generate multiple beamlets and interference patterns consists of an AOF cavity and two converging lenses. In the focal plane of the first lens, the AOF cavity diffracts the incident Gaussian beam (top) into multiple beamlets (middle) that, after passing through the second lens, interfere, forming a light pattern (bottom). The beamlets and interference in the figure were generated at the acoustic frequencies of 1.37 MHz and 1.8 MHz, respectively. Scale bars are 200 μm.

The AOF system also enables more complex light shaping. Specifically, after passing through the second converging lens, the diffracted beamlets interfere, generating an intensity pattern. Notably, the generated pattern can be controlled with the same parameters that control the beamlets. The phase, in particular, allows ultra-fast pattern selection when a pulsed laser with a duration much smaller than the temporal period of the driving signals is used [32], [33]. In this case, the laser pulse interacts with an instantaneous refractive index profile (see Equation 2) that can be selected by delaying the arrival of the laser with respect to the temporal period of the driving signal and, thus, with nanosecond resolution. In this configuration, the AOF system can boost the throughput of an LDW machine by scanning the material surface region-by-region rather than point-by-point.

3. CYBER-PHYSICAL SYSTEM FOR LASER MANUFACTURING

Figure 3 a) schematically describes the architecture of a laser-based cyber-physical workstation with AOF functionalities. The station is organised in two levels: physical and digital. The former handles the operations that are necessary for the manufacturing of the workpiece and is connected to the digital one through a network (a private network in the current setup), which provides the physical world with access to various users, computers, and data-storage systems. The mutual interaction between these levels results into a cyber-physical system in which information and actions can be monitored and synchronised between the "factory floor" and cyberspace. For instance, the digital level can collect data from the physical objects that, once processed, can be used to monitor the manufacturing process, compute the usage or wear of a physical object, or tag a workpiece.
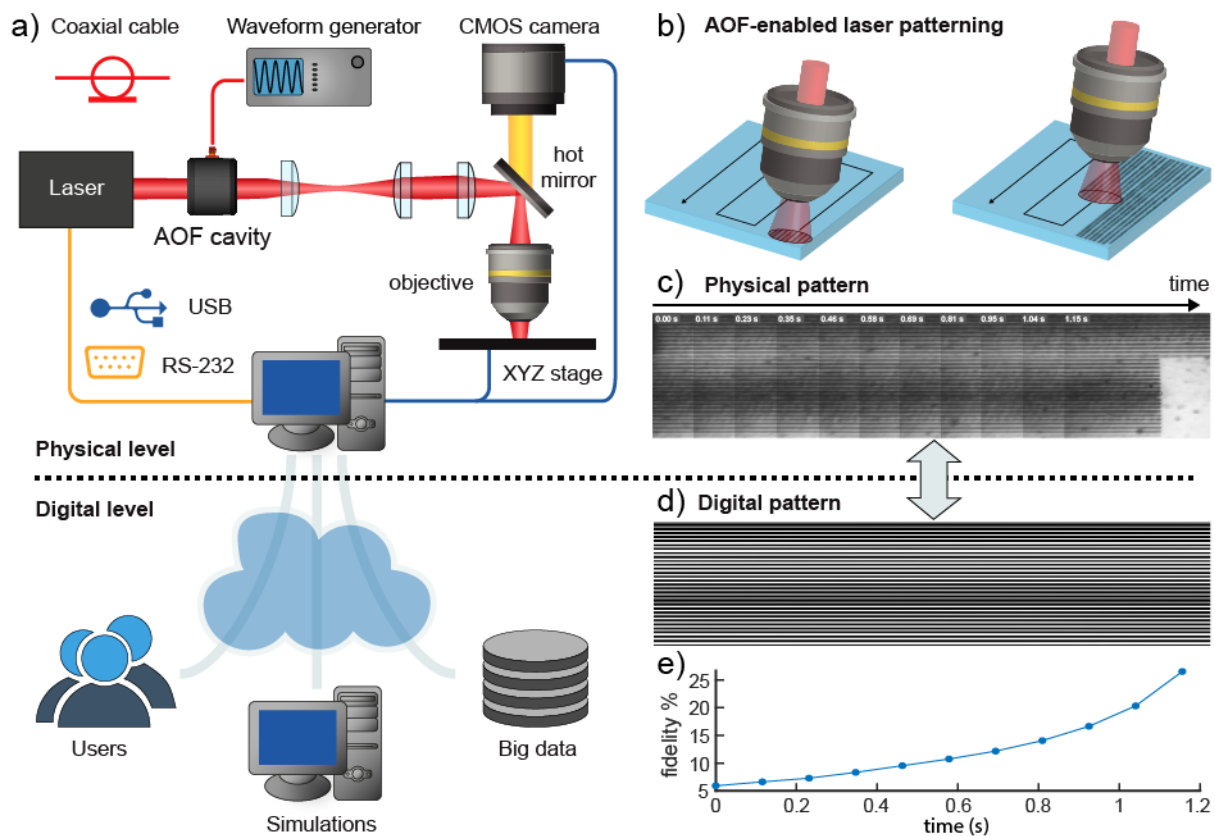
Figure 3. Cyber-physical system for AOF-enabled laser manufacturing. a) The architecture of the laser-based CPS comprises a physical (top) and digital (bottom) level. The former consists of an LDW station integrating an AOF cavity that is conjugated with the plane of the workpiece by means of a series of converging lenses. The physical and digital levels are connected through a network that offers access to the AOF-LDW station to users, workstations, or data-storage devices. B–e) Digital assessment of the workpiece fidelity. b) Schematic description of the strategy used for large-area patterning with an AOF-shaped laser beam. c) Large field-of-view image of the ablated pattern. d) Digital copy of the target pattern. e) Fidelity between the physical and digital patterns at different time steps.

3.1. Implementation of the physical space of a laser-based CPS

The physical part of a laser-based cyber-physical system comprises several elements. The key component is an LDW station that consists of an ultrafast pulsed laser emitting 70-fs pulses at an operational wavelength of 800 nm, an upright microscope equipped with a long working-distance microscope objective (numerical aperture 0.55), a complementary metal–oxide–semiconductor (CMOS) camera for real-time inspection of the workpiece, and an AOF cavity. A waveform generator provides the driving signals for proper AOF operation. For laser manufacturing using the interference patterns, the AOF cavity is conjugated to the workpiece plane by means of relay lenses. Simply removing one of these lenses enables the generation of multiple diffracted spots at the focal plane of the microscope objective. In both cases, high-throughput material processing can be achieved by using a motorised XYZ stage to displace the sample relative to the acoustically shaped light (see Figure 3 b). Complex patterns can be prepared by varying the resonances, i.e. by controlling the driving parameters while scanning the sample surface.

3.2. Digital assessment of the AOF-generated pattern fidelity

The proof of concept for the computational operations of the digital level of the laser-based CPS is provided by successfully monitoring the fidelity between a physical pattern and its digital avatar. In this experiment, we ablated a large-area pattern onto a chromium substrate by scanning its surface with up to 19 AOF-generated beamlets and using a CMOS camera to record the machining process. Figure 3 c) shows an optical image of a fraction of the physical pattern that was obtained by stitching together 11 frames of the recorded video. The corresponding digital counterpart (a binary pattern in this case) is shown in Figure 3 d). At each time step, we used cross-correlation to evaluate the fidelity or similarity between the instantaneous physical pattern and the final digital copy. As shown in Figure 3 e), initially ($t = 0$), the fidelity is 0 because the physical pattern does not yet exist and it increases at each time step as soon as the ablation proceeds, indicating that the laser-machining process is performing well. Notably, deviation from the expected trend can be used to predict errors or the failure of one or more physical objects in the LDW station.

Our results clearly prove that the functionalities of the AOF-LDW station can be augmented by collecting data from the physical space and using it to monitor the similarity between the machined workpiece and its digital copy. In the future, the digital pattern could be decomposed into fundamental patterns, for instance, by means of Fourier transformation, in order to directly provide the AOF system with suitable driving parameters. In conjunction with appropriate XYZ scanning, this strategy will enable the realisation of totally automatised and digitally controlled laser-based machining tools.

As we implement more computational operations and improve data collection capabilities at the physical level, with sensors or advanced imaging methods, interesting possibilities will continue to emerge, providing novel opportunities for laser machining tool development and optimisation.

4. MATERIAL PROCESSING WITH THE AOF-LDW STATION

The previous sections demonstrate that AOF technology can be effectively integrated into an LDW station and then into a cyber-physical system. What remains is proving if the AOF technology enables high-throughput laser manufacturing. To answer this question, we used the AOF-LDW to machine several materials (metals, semiconductors, and polymers) in both additive and subtractive mode.

Figure 4 shows two examples of subtractive laser manufacturing of semiconductors and metals, e.g. patterns ablated in silicon [Figure 4. a)] and palladium [Figure 4. b)]. For the ablation of Si, we used both piezoelectric couples of the AOF cavity to generate a 2D distribution of the diffracted beamlets. In detail, driving the piezoelectric plates at the resonant frequency of $f_r = 4.5$ MHz led to a 5-fold enhancement in the throughput of the manufacturing process. Alternatively, for the ablation of palladium, we used only one axis of the AOF cavity, which we modulated between the ON and OFF states while snake-scanning the sample surface. This strategy resulted in a more complex pattern and a 9-fold enhancement (in the ON state) in the throughput of the laser ablation.

As shown in Figure 5, the AOF-LDW station also allows for the machining of an entire area with single-laser irradiation when interference patterns are used. We tested this functionality in both additive [Figure 5 a) and b)] and subtractive [Figure 5 c) and d)] modes. Figure 5 a) in particular shows photo-polymerised structures formed by scanning an epoxy resin along the X-axis with an intensity pattern generated at an acoustic frequency of 1.2 MHz. To increase the complexity of the polymeric structures, we exploited the binary modulation (ON–OFF and vice versa)
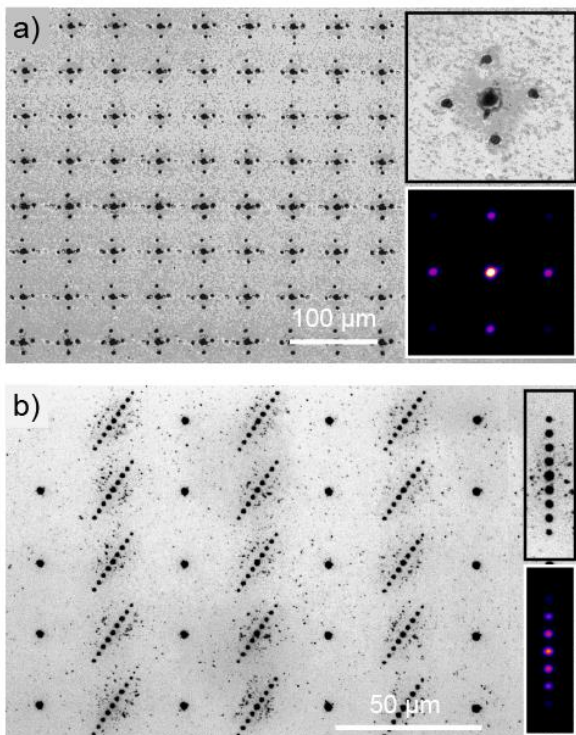
Figure 4. Laser material processing with multiple beamlets. a) Optical image of a pattern ablated into silicon with a beamlet distribution obtained by driving the X- and Y-axis of the AOF cavity at the same resonant frequency. b) Laser ablation of a chromium substrate generated by snake scanning the sample surface while the AOF cavity was alternating between the ON and OFF states. The insets show a magnified view of the patterns, ablated with a single laser irradiation and corresponding laser intensity distributions.

of the AOF cavity while snake-scanning the resin. Figure 5 b) shows a 3D map of a representative portion of the photo-polymerised structures that highlights the high quality of the prepared surfaces without evident defects or irregularities.

Figure 5 c) shows an example of a metallic pattern that we obtained with the laser-ablation of a palladium substrate. In this experiment, the substrate surface was snake-scanned with two alternating interference patterns generated by driving a single piezoelectric pair at the acoustic frequencies of 1.2 MHz and 1.8 MHz, respectively. This strategy resulted in two closely periodic microstructures (aligned with the interference pattern) with periods of 2.1 µm and 2.9 µm, respectively. Interestingly, the atomic force microscopy (AFM) measurements in Figure 5 d), on a fraction of these structures, reveal the existence of periodic nanoripples (width ~ 250 nm and period ~ 500 nm) orthogonal to the interference pattern. Also known as laser-induced periodic surface structures or LIPSS, they are of great interest for industrial applications such as structural coloration, control of surface wetting, engineering bacterial and cellular proliferation on substrates, and optimisation of the tribology of a surface [35]-[39].

5. CONCLUSION

An AOF-LDW system is a feasible and functional machine tool for I4. In particular, the high speed and versatility, in terms of beam shaping, offered by the AOF cavity enables high-throughput laser manufacturing of various materials of industrial interest with both additive and subtractive functionality. The shape of the laser beam depends on the amplitude, frequency, and phase of the oscillating refractive index of the liquid in the cavity. As such, rapid pattern selection is possible by simply adjusting the driving signals. As our results demonstrate, integrating the AOF cavity into an LDW station is simple, and, with few optical elements (lenses), either beam parallelisation or the generation of an interference pattern can be selected. The AOF-LDW station is digitally controlled and can be connected to cyberspace, enabling the realisation of a laser-based cyber-physical system with advanced manufacturing functionalities.

We can anticipate that in conjunction with the use of intelligent systems [40] and improved wireless connections, the AOF-enabled cyber-physical system will enable the realisation of autonomous manufacturing tools that adapt their operations in response to feedback, collected data, or their own learning abilities.

6. APPENDIX – MATERIALS AND METHODS

6.1. Optical Characterisation Setup

Light intensity distributions produced with the AOF cavity were recorded with a CMOS camera (ThorLabs, DCC1545M) placed after the lens system used to generate either beamlets or interference patterns. A 445 nm laser was used in this experiment (Coherent CUBE 445-40C).

6.2. Laser Polymerisation

Pentaerythritol triacrylate and isopropylthioxanthone were purchased from Sigma-Aldrich and used as a negative resin and photo initiator, respectively. Photopolymerisation was induced by scanning the resin with an AOF-generated interference patter with a dose of 0.3 µJ per pulse. To remove the uncured resin, the sample was immersed in methanol for five minutes and then rinsed with isopropanol.
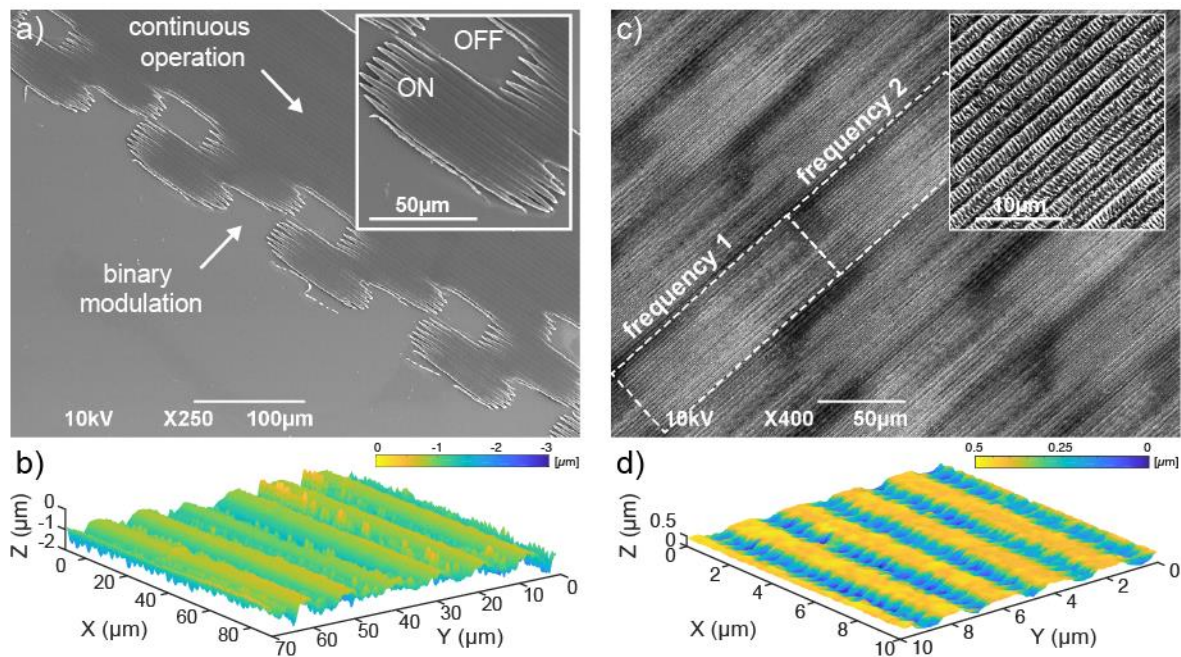
Figure 5. Laser material processing with intensity patterns. a) Scanning electron micrograph (SEM) of polymeric microstructures obtained by snake scanning an epoxy resin with an interference pattern generated at the acoustic frequency of 1.2 MHz. Alternating the AOF cavity between the ON and OFF states causes the polymerisation of complex structures. The inset highlights the high quality of the polymerised surfaces. This is further confirmed by the 3D map acquired with an optical profilometer, as shown in b). c) Scanning electron micrograph of a pattern with two distinct regions obtained by snake scanning a palladium substrate while alternating the acoustic frequency between 1.2 and 1.8 MHz. The magnified SEM image reveals the presence of nanoripples in the laser-irradiated regions, as confirmed by the AFM measurements shown in d).

6.3. Sample Characterisation

Laser-modified materials were inspected with a scanning electron microscope (JSM-6390, JEOL) at an acceleration voltage of 10 kV. Polymeric samples were sputter-coated with 10 nm of gold to inhibit charging effects. The height map of the polymeric structures was measured with an optical profilometer (Zeta-20, Zeta Instruments). The morphology of the metal surfaces was imaged with an atomic force microscope (MFP-3D, Asylum Research) operating in tapping mode in air. The probes (PPP-NCHR, Nanosensors) were aluminium-coated Si cantilevers with a resonance frequency of 330 kHz, spring constant of 40 N m^{-1}, and tip-radius of 5 nm. Amplitude images were collected by scanning 10×10 μm^2 areas with a resolution of 256×256 pixels.

6.4. Measurement of the Transfer Function

To acquire the amplitude and phase of the transfer function of the resonant cavity, a sinusoidal signal was applied to one of the piezoelectric plates (transmitters) while acquiring the signal of the opposed plate (receiver) with an oscilloscope. A sinusoidal function was fitted to both recorded signals to measure both their amplitude ratio, A_R/A_T, and phase shift, $\phi_R - \phi_T$. The transfer function was obtained by sweeping the frequency of the driving signal in the interval of 0.99–1.015 MHz.

REFERENCES

[1] M. C. F. Souza, M. Sacco, A. J. V. Porto, Virtual manufacturing as a way for the factory of the future, J. Intell. Manuf. 17 (2006), pp. 725-735.
DOI: https://doi.org/10.1007/s10845-006-0041-1

[2] P. Zheng, H. Wang, Z. Sang, R. Y. Zhong, Y. Liu, C. Liu, K. Mubarok, S. Yu, X. Xu, Smart manufacturing systems for Industry 4.0: Conceptual framework, scenarios, and future perspectives, Front. Mech. Eng. 13 (2018), pp. 137-150.
DOI: https://doi.org/10.1007/s11465-018-0499-5

[3] W. Viriyasitavat, T. Anuphaptrirong, D. Hoonsopon, When blockchain meets Internet of Things: Characteristics, challenges, and business opportunities, J. Ind. Inf. Integr. 15 (2019), pp. 21-28.
DOI: https://doi.org/10.1016/j.jii.2019.05.002

[4] W. Peng, Y. Chen, W. Ai, Higher-order mode photonic crystal based nanofluidic sensor, Opt. Commun. 382 (2017), pp. 105-112.
DOI: https://doi.org/10.1016/j.optcom.2016.07.019

[5] L. Angrisani, U. Cesaro, M. D'Arco, O. Tamburis, Measurement applications in Industry 4.0: The case of an IoT-oriented platform for remote programming of automatic test equipment, Acta Imeko 8 (2019) 2, pp. 62-69. Online [Accessed 08 December 2020]
https://acta.imeko.org/index.php/acta-imeko/article/view/IMEKO-ACTA-08%20%282019%29-02-09

[6] T. Addabbo, A. Fort, M. Mugnaini, L. Parri, S. Parrino, A. Pozzebon, V. Vignoli, A low power IoT architecture for the monitoring of chemical emissions, Acta Imeko 8 (2019), pp. 53-61. Online [Accessed 08 December 2020]
https://acta.imeko.org/index.php/acta-imeko/article/view/IMEKO-ACTA-08%20%282019%29-02-08

[7] A. Cilfone, L. Davoli, L. Belli, G. Ferrari, Wireless mesh networking: An IoT-oriented perspective survey on relevant technologies, Futur. Internet 11 (2019), 99, 35 pages.
DOI: https://doi.org/10.3390/fi11040099

[8] M. A. Siddiqi, H. Yu, J. Joung, 5G ultra-reliable low-latency communication implementation challenges and operational issues with IoT devices, Electron. 8 (2019), 981, 18 pages.
DOI: https://doi.org/10.3390/electronics8090981

[9] S. Choudhury, P. Kuchhal, R. Singh, A. Gehlot, ZigBee and bluetooth network based sensory data acquisition system,

Procedia Comput. Sci. 48 (2015), pp. 367-372.
DOI: https://doi.org/10.1016/j.procs.2015.04.195

[10] X. Xu, Machine tool 4.0 for the new era of manufacturing, Int. J. Adv. Manuf. Technol. 92 (2017), pp. 1893-1900.
DOI: https://doi.org/10.1007/s00170-017-0300-7

[11] G. Fazzini, P. Paolini, R. Paolucci, D. Chiulli, G. Barile, A. Leoni, M. Muttillo, L. Pantoli, G. Ferri, Print On Air: FDM 3D Printing Without Supports, in: 2019 II Workshop Metrol. Ind. 4.0 IoT (MetroInd4.0&IoT), Naples, Italy, 4-6 June 2019: pp. 350-354.
DOI: https://doi.org/10.1109/METROI4.2019.8792846

[12] T. D. Ngo, A. Kashani, G. Imbalzano, K. T. Q. Nguyen, D. Hui, Additive manufacturing (3D printing): A review of materials, methods, applications and challenges, Composites Part B Eng. 143 (2018), pp. 172-196.
DOI: https://doi.org/10.1016/j.compositesb.2018.02.012

[13] J. M. Flynn, A. Shokrani, S. T. Newman, V. Dhokia, Hybrid additive and subtractive machine tools – Research and industrial developments, Int. J. Mach. Tools Manuf. 101 (2016), pp. 79-101.
DOI: https://doi.org/10.1016/j.ijmachtools.2015.11.007

[14] C. B. Arnold, P. Serra, A. Piqué, Laser direct-write techniques for printing of complex materials, MRS Bull. 32 (2007), pp. 23-31.
DOI: https://doi.org/10.1557/mrs2007.11

[15] M. Schmidt, M. Merklein, D. Bourell, D. Dimitrov, T. Hausotte, K. Wegener, L. Overmeyer, F. Vollertsen, G. N. Levy, Laser based additive manufacturing in industry and academia, CIRP Ann. 66 (2017), pp. 561-583.
DOI: https://doi.org/10.1016/j.cirp.2017.05.011

[16] N. T. Aboulkhair, M. Simonelli, L. Parry, I. Ashcroft, C. Tuck, R. Hague, 3D printing of aluminium alloys: Additive manufacturing of aluminium alloys using selective laser melting, Prog. Mater. Sci. 106 (2019), pp. 1-45.
DOI: https://doi.org/10.1016/j.pmatsci.2019.100578

[17] Y. Hu, W. Cong, A review on laser deposition-additive manufacturing of ceramics and ceramic reinforced metal matrix composites, Ceram. Int. 44 (2018), pp. 20599-20612.
DOI: https://doi.org/10.1016/j.ceramint.2018.08.083

[18] S. Surdo, S. Piazza, L. Ceseracciu, A. Diaspro, M. Duocastella, Towards nanopatterning by femtosecond laser ablation of pre-stretched elastomers, Appl. Surf. Sci. 374 (2015), pp. 151-156.
DOI: https://doi.org/10.1016/j.apsusc.2015.10.142

[19] C. Leone, V. Lopresto, I. De Iorio, Wood engraving by Q-switched diode-pumped frequency-doubled Nd:YAG green laser, Opt. Lasers Eng. 47 (2009), pp. 161-168.
DOI: https://doi.org/10.1016/j.optlaseng.2008.06.019

[20] A. Stepanov, M. Manninen, I. Pärnänen, M. Hirvimäki, A. Salminen, Laser cutting of leather: Tool for industry or designers?, Phys. Procedia. 78 (2015), pp. 157-162.
DOI: https://doi.org/10.1016/j.phpro.2015.11.028

[21] S. Surdo, A. Diaspro, M. Duocastella, Microlens fabrication by replica molding of frozen laser-printed droplets, Appl. Surf. Sci. 418 (2017), pp. 554-558.
DOI: https://doi.org/10.1016/j.apsusc.2016.11.077

[22] T. DebRoy, H. L. Wei, J. S. Zuback, T. Mukherjee, J. W. Elmer, J. O. Milewski, A. M. Beese, A. Wilson-Heid, A. De, W. Zhang, Additive manufacturing of metallic components – Process, structure and properties, Prog. Mater. Sci. 92 (2018), pp. 112-224.
DOI: https://doi.org/10.1016/j.pmatsci.2017.10.001

[23] F. Vollertsen, M. Grupp, Laser beam joining of dissimilar thin sheet materials, Steel Res. Int. 76 (2005), pp. 240-244.
DOI: https://doi.org/10.1002/srin.200506003

[24] T. Deng, J. Li, Z. Zheng, Fundamental aspects and recent developments in metal surface polishing with energy beam irradiation, Int. J. Mach. Tools Manuf. 148 (2020), 103472.
DOI: https://doi.org/10.1016/j.ijmachtools.2019.103472

[25] J. D. Yao, Z. Q. Zheng, G. W. Yang, Production of large-area 2D materials for high-performance photodetectors by pulsed-laser deposition, Prog. Mater. Sci. 106 (2019) 100573.
DOI: https://doi.org/10.1016/j.pmatsci.2019.100573

[26] A. J. López, J. Lamas, J. S. Pozo-Antonio, T. Rivas, A. Ramil, Development of processing strategies for 3D-controlled laser ablation: Application to the cleaning of stonework surfaces, Opt. Lasers Eng. 126 (2020), 105897.
DOI: https://doi.org/10.1016/j.optlaseng.2019.105897

[27] L. Kelemen, S. Valkai, P. Ormos, Parallel photopolymerisation with complex light patterns generated by diffractive optical elements, Optics Express 15 (2007) 14488.
DOI: https://doi.org/10.1364/OE.15.014488

[28] S. Alamri, M. El-Khoury, A. I. Aguilar-Morales, S. Storm, T. Kunze, A. F. Lasagni, Fabrication of inclined non-symmetrical periodic micro-structures using direct laser interference patterning, Sci. Rep. 9 (2019), pp. 1-12.
DOI: https://doi.org/10.1038/s41598-019-41902-x

[29] S. Beke, B. Farkas, I. Romano, F. Brandi, 3D scaffold fabrication by mask projection excimer laser stereolithography, Opt. Mater. Express 4 (2014), pp. 2032-2041.
DOI: https://doi.org/10.1364/OME.4.002032

[30] J. Cheng, C. Gu, D. Zhang, S.-C. Chen, High-speed femtosecond laser beam shaping based on binary holography using a digital micromirror device, Opt. Lett. 40 (2015) 21, pp. 4875-4878.
DOI: https://doi.org/10.1364/OL.40.004875

[31] J. Li, Y. Tang, Z. Kuang, J. Schille, U. Loeschner, W. Perrie, D. Liu, G. Dearden, S. Edwardson, Multi imaging-based beam shaping for ultrafast laser-material processing using spatial light modulators, Opt. Lasers Eng. 112 (2019), pp. 59-67.
https://doi.org/10.1016/j.optlaseng.2018.09.002

[32] A. Zunino, S. Surdo, M. Duocastella, Dynamic multifocus laser writing with acousto-optofluidics, Adv. Mater. Technol. 4 (2019), 1900623.
DOI: https://doi.org/10.1002/admt.201900623

[33] S. Surdo, M. Duocastella, Fast acoustic light sculpting for on-demand maskless lithography, Adv. Sci. 9 (2019), 1900304.
DOI: https://doi.org/10.1002/advs.201900304

[34] E. McLeod, C. B. Arnold, Mechanics and refractive power optimization of tunable acoustic gradient lenses, J. Appl. Phys. 102 (2007), 033104, 10 pages.
DOI: https://doi.org/10.1063/1.2763947

[35] I. Gnilitskyi, T. J. Y. Derrien, Y. Levy, N. M. Bulgakova, T. Mocek, L. Orazi, High-speed manufacturing of highly regular femtosecond laser-induced periodic surface structures: Physical origin of regularity, Sci. Rep. 7 (2017), pp. 1-11.
DOI: https://doi.org/10.1038/s41598-017-08788-z

[36] F. A. Müller, C. Kunz, S. Gräf, Bio-inspired functional surfaces based on laser-induced periodic surface structures, Materials (Basel), 9 (2016), pp. 476.
DOI: https://doi.org/10.3390/ma9060476

[37] S. van der Poel, M. Mezera, G. Römer, E. de Vries, D. Matthews, Fabricating laser-induced periodic surface structures on medical grade cobalt–chrome–molybdenum: Tribological, wetting and leaching properties, Lubricants 7 (2019), 70, 14 pages.
DOI: https://doi.org/10.3390/lubricants7080070

[38] I. Gnilitskyi, M. Pogorielov, R. Viter, A. M. Ferraria, A. P. Carapeto, O. Oleshko, L. Orazi, O. Mishchenko, Cell and tissue response to nanotextured Ti6Al4V and Zr implants using high-speed femtosecond laser-induced periodic surface structures, Nanomedicine Nanotechnology, Biol. Med. 21 (2019), 102036.
DOI: https://doi.org/10.1016/j.nano.2019.102036

[39] F. Carpignano, G. Silva, S. Surdo, V. Leva, A. Montecucco, F. Aredia, A. I. Scovassi, S. Merlo, G. Barillaro, G. Mazzini, A new cell-selective three-dimensional microincubator based on silicon photonic crystals, Plos ONE 7 (2012), 48556.
DOI: https://doi.org/10.1371/journal.pone.0048556

[40] W. Liu, C. Kong, Q. Niu, J. Jiang, X. Zhou, A method of NC machine tools intelligent monitoring system in smart factories, Robot. Comput. Integr. Manuf. 61 (2020), 101842.
DOI: https://doi.org/10.1016/j.rcim.2019.101842